KEK Preprint 95-10
April 1995
H

CERN LIBRARIES, GENEVA
SCAN-9507097

SW 9529

Hypernuclear Weak Decay of ${}^{12}_{\Lambda}C$ and ${}^{11}_{\Lambda}B$

H. NOUMI, S. AJIMURA, H. EJIRI, A. HIGASHI, T. KISHIMOTO,
D.R. GILL, L. LEE, A. OLIN, T. FUKUDA and O. HASHIMOTO

Submitted to Phys. Rev. C.

National Laboratory for High Energy Physics, 1995

KEK Reports are available from:

Technical Information & Library
National Laboratory for High Energy Physics
1-1 Oho, Tsukuba-shi
Ibaraki-ken, 305
JAPAN

Phone: 0298-64-1171
Telex: 3652-534 (Domestic)
(0)3652-534 (International)
Fax: 0298-64-4604
Cable: KEK OHO
E-mail: LIBRARY@JPNKEKVX (Bitnet Address)
library@kekvax.kek.jp (Internet Address)

Hypernuclear Weak Decay of ${}^{12}_{\Lambda}C$ and ${}^{11}_{\Lambda}B$

H. Noumi[1], S. Ajimura, H. Ejiri[2], A. Higashi[3], and T. Kishimoto

Department of Physics, Faculty of Science
Osaka University, Toyonaka, Osaka 560, JAPAN

D. R. Gill, L. Lee, and A. Olin

TRIUMF, Vancouver, BC, CANADA V6T 2A3

T. Fukuda, and O. Hashimoto

Institute for Nuclear Study
University of Tokyo, Tanashi, Tokyo 188, JAPAN

Abstract

The branching ratios of negative pions and protons due to the weak decays of ${}^{12}_{\Lambda}C$ and ${}^{11}_{\Lambda}B$ hypernuclei were measured. The negative pionic decay rates (Γ_{π^-}), proton-induced nonmesonic decay rates (Γ_p), total nonmesonic decay rates (Γ_{nm}) and ratios of the $\Lambda n \rightarrow nn$ process to the $\Lambda p \rightarrow pn$ process (Γ_n/Γ_p) were derived from the present measurements combined with previous studies on the mesonic π^0 and total decay rates. The measured Γ_{π^-} shows that Pauli blocking is less effective than expected due to pion distortion. We found that Γ_{nm} is nearly equal to unity in units of the free-space Λ-decay width. The present results also indicate that Γ_n is almost twice that of Γ_p. This is in disagreement with calculations based on meson-exchange models in which Γ_n is strongly suppressed.

[1]present address : *National Laboratory for High Energy Physics, Tsukuba, Ibaraki 305, JAPAN*
[2]present address : *Research Center for Nuclear Physics, Osaka University, Ibaraki, Osaka 567, JAPAN*
[3]present address : *Institute for Nuclear Study, University of Tokyo, Tanashi, Tokyo 188, JAPAN*

I. INTRODUCTION

In single Λ hypernuclei a Λ hyperon is free from the Pauli exclusion principle which governs nucleons because it has a different quantum number, strangeness ($S \neq 0$). Consequently, the Λ can occupy any orbital in the hypernucleus. In general, the excited hypernucleus is stable against Λ emission and decays into the ground state by emitting nucleons and/or γ rays. It eventually decays by weak processes. The decay properties reflect the dynamics of the hyperon and the nucleons in the hypernucleus. We can learn through studies of hypernuclear weak decays how real/virtual bosons propagate and how baryons/quarks correlate in the nuclear medium. However, experimental data on hypernuclear weak decays is limited, and there remain many questions. It is of particular importance to accumulate higher quality data to constrain the various theoretical models put forth.

A hypernucleus decays in two predominant hadronic weak processes, which are characterized by the following elementary processes:

$$\text{M-decay} \quad \Lambda \rightarrow p + \pi^-, n + \pi^0 \quad \Delta q \sim 100 \text{ MeV/c}, \tag{1}$$
$$\text{NM-decay} \quad \Lambda + N \rightarrow p + n, n + n \quad \Delta q \sim 400 \text{ MeV/c}. \tag{2}$$

Mesonic decay (M-decay) is well known through studies of nonleptonic-Λ decays in free space. M-decay can be used as a good tool to identify hypernuclei and to determine the spin of hypernuclei. M-decay is suppressed in hypernuclei with $A \geq 7$ due to Pauli blocking effects because the momentum transfer, $\Delta q \sim 100$ MeV/c, is much smaller than the Fermi momentum of ~250 MeV/c. The suppression of the M-decay rates (Γ_{π^-}, Γ_{π^0}) is reduced by the ΛN many-body interaction and by a distortion of the pion wave in the nuclear medium [1, 2]. Systematic studies of the M-decay rates are of interest.

Nonmesonic decay (NM-decay) predominates in hypernuclei, except for light hypernuclei. It provides a unique opportunity to investigate the ΛN weak interaction since the transition $\Lambda N \rightarrow NN$ can take place only in the nucleus. The NM-decay rates, Γ_p (proton-induced decay rate) and Γ_n (neutron-induced decay rate), are good observables through which the decay mechanism can be clarified. Until now, no theoretical calculations based on meson-exchange models can reproduce the experimental measurements on the NM-decay rates, particularly on the ratio of Γ_n to Γ_p [3, 4, 5]. It has recently been suggested [6] that the discrepancy between theory and experiment may be explained by multinucleon-induced processes, such as $\Lambda NN \rightarrow NNN$, although this has not yet been established very well.

In recent years a series of counter experiments carried out at BNL measured a set of weak decay rates, the lifetime (τ=$1/\Gamma_{tot}$) and the partial rates (Γ_{π^-}, Γ_p, and Γ_n), in ${}^{5}_{\Lambda}He$, ${}^{11}_{\Lambda}B$ and ${}^{12}_{\Lambda}C$ produced via (K^-, π^-) reactions [7, 8]. Before the BNL measurements the experimental data were limited to those from old emulsion and bubble-chamber experiments, where identification of hypernuclei was difficult, except for very light hyperfragments. The counter experiments improved the quality of data very much. However, only the lifetimes could be obtained for ${}^{11}_{\Lambda}B$ and ${}^{12}_{\Lambda}C$ because a large background from in-flight kaon decays contaminated the hypernuclear excitation-energy spectrum. Therefore, an improvement of this measurement is desired.

We recently carried out an experiment to study the polarizations and weak decays of hypernuclei produced via (π^+, K^+) reactions on ${}^{12}C$ at KEK (PS E160) [9]. In the present work we report on the weak decay rates of ${}^{12}_{\Lambda}$C and ${}^{11}_{\Lambda}$B. The asymmetry of the weak decays and polarizations have been presented elsewhere [10].

II. EXPERIMENTAL SETUP

The present experiment was carried out at the K2 beam line [11] of the KEK 12-GeV Proton Synchrotron (PS). We constructed the PIK spectrometer in order to study hypernuclei produced via (π^+, K^+) reactions in the previous experiment [12]. For the present experiment, decay counter telescopes were installed in the PIK spectrometer, as shown in Fig. 1. A platinum target of 6 mm in diameter and 60 mm in length was irradiated with typically 2.5×10^{12} protons from the KEK PS every 4 seconds (spill interval) with a duty factor of 50%, producing secondary pions. About 5×10^6 positive pions per spill at a momentum of 1.05 GeV/c were delivered to the experimental target through the K2 beam line. The pion beam was defined by a coincidence between beam hodoscopes BH1 and BH2. The K2 beam line provided a clean beam of pions via a static separator 6 m long operating at an electric field of 40 kV/cm. Less than a 20% positron contamination was found in the pion beam. These were rejected by anti-coincidence with a gas Čerenkov counter (GČ) located before BH1. A plastic scintillator was employed as an active target (TGT). It had dimensions of 60(wide)×20(high)×64(long) mm³, and was divided into two halves in height and 32 segments in length to obtain dE/dx information near to the reaction vertex [13]. Differential lucite Čerenkov counters (BLČ's) were used to discard beam pions passing through, but not interacting with, the target. Scattered particles were triggered by a scintillator hodoscope (TOF) located behind the PIK-PA spectrometer. Scattered kaons were triggered by a proper combination of two Čerenkov detectors, LČ and AČ. The LČ array consisted of 11 slabs of lucite Čerenkov radiator with wavelength shifter. The AČ comprised aerogel Čerenkov radiators with a refractive index of $n\sim1.055$. The trigger condition for the (π^+, K^+) reaction was then defined by

$$\pi K = BH1 * \overline{G\check{C}} * BH2 * TGT * \overline{BL\check{C}} * TOF * L\check{C} * \overline{A\check{C}}.$$

Drift chambers BDC1∼5 and SDC1∼4 were tracking detectors for the incident beam pions and the scattered kaons, respectively. They were used to reconstruct particle momenta ($\boldsymbol{k}_{\pi^+}$ and $\boldsymbol{k}_{K^+}$). The BDC's, SDC1 and SDC2 were drift chambers with a narrow drift space of 2.5 mm, so that they could be operated in a high-intensity beam of more than 10^6 particles per second. Drift chambers SDC3 and SDC4 were used to detect scattered particles, and were large enough to cover the solid angle of the PIK-PA spectrometer. Since the PIK-PA spectrometer had a large momentum acceptance (0.5∼0.9 GeV/c), energetic protons with velocities close to that of kaons contaminated the trigger. Scattered kaons were clearly distinguished from the background particles by means of mass reconstruction from the measured momentum and time-of-flight between BH2 and the TOF array in an off-line analysis. Fig. 2 shows the mass reconstruction. The proton mass was slightly shifted because the velocity-reconstruction function from the time-of-flight was optimized for kaons.

Decay particles from the hypernuclei were detected by two sets of decay counter telescopes located above and below the target. Each counter telescope set comprised an array of ΔE and E counters. The E counter comprised 16 NaI detectors, each with a volume of 82×82×76 mm³. The ΔE counter comprised 4 slabs of 5 mm thick plastic scintillators located in front of the E counters. Charged decay particles were identified by the ΔE counter.

Protons and negative pions from decaying hypernuclei were identified with the particle-identification (PI) function, defined by

$$F_{PI} = a \ln \Delta E + b \ln E_t, \quad (3)$$

where $E_t(=\Delta E + E)$ is the total energy deposited in the decay counter telescopes. Coefficients a and b are ~ 0.8 and ~ 1.0, respectively, which were determined by the Bethe-Bloch equation. Fig. 3 illustrates a typical PI spectrum for decay particles of $E_t > 25$ MeV. The pion and proton windows were set in the PI spectrum as shown in the figure. A small fraction of pions contaminated in the proton-gated spectrum due to impurities in the PI proton window. Similarly, the pion-gated spectrum was contaminated by the protons. The fraction of pions in the proton window to pions in the pion window was estimated to be 3.5% by extrapolating the curves, as shown in the figure. In the same manner, the fraction of protons in the pion window to protons in the proton window was found to be 6.0%.

In order to reduce the computer dead time the unbiased πK trigger was prescaled by a factor of 2. Event candidates ($EVENT$) were kept when they satisfied the condition
(i) prescaled πK or
(ii) a decay event ($DECAY$) in coincidence with πK.
A decay event was triggered if at least one NaI detected a particle from the target. The prescaled (π^+, K^+) events and the $DECAY$ events were distinguished by labeling each event via a coincidence register.

Signals from the detectors were digitized by ADC's and TDC's and were accumulated in CAMAC memory modules waiting to be read out by the data-acquisition computer. Data transfer to the computer occurred before the memory modules became filled with data. With an event size of around 600 bytes, the memory modules could accept about 30 events in the present experiment. The event rate was 60∼80 per spill, and the computer trigger rate was a few per spill. The computer dead time was as small as 10%.

III. ANALYSES AND RESULTS

A. Hypernuclear Excitation Spectra

Fig. 4 illustrates the hypernuclear excitation-energy spectra obtained using the active target. Fig. 4-a shows the (π^+, K^+) singles spectrum prescaled by a factor of 2, and Figs. 4-b and 4-c are the spectra in coincidence with decay protons and pions, respectively. A peak in the ground-state region can be seen at $E_x \sim 0$ MeV. The energy resolution of $\sigma \sim 3$ MeV is principally due to the target thickness (6.6 g/cm²). The first excited state ($E_x \sim 10$ MeV) as well as the ground state are enhanced in the p-gated spectrum, since the NM-decay probability is suppressed in the Λ-unbound region ($E_x > 11$ MeV), and are sufficiently clear to obtain a yield for each peak.

The ground and first-excited states correspond to the n-hole Λ-particle states of $[p^{-1}s_\Lambda]$ and $[p^{-1}p_\Lambda]$, respectively. A calculation [14] indicates that the (π^+, K^+) reaction mainly populates the 1^- and 2^+ states in the ground and the first-excited states of ${}^{12}_{\Lambda}C$, respectively. These states have been well established through studies of hypernuclear production at CERN, BNL and KEK [12, 15, 16]. We thus assumed in the fitting procedure to extract the peak yields that two Gaussian peaks with $\sigma \sim 3$ MeV are located at $E_x = 0$ MeV and $E_x = 10$ MeV.

The region above $E_x \sim 11$ MeV is open for the Λ-escape channel (Λ-unbound region). To reproduce the spectrum shape of this continuum region we used the calculated states from ref. [17]. Each state was folded with a Gaussian resolution function of $\sigma \sim 3$ MeV in the present fitting procedure (FIT-1). Even in this region, a certain fraction of the states may form a hyperfragment through the Λ-spreading process [18]. These are characterized by the compound process, where the intermediate state populated by the reaction decays into a daughter nucleus statistically. Since the hyperfragments can emit protons through NM-decays the same fitting procedure could be used for the p-gated spectrum.

In a separate fitting procedure we assumed that the spectrum shape in the Λ-unbound region could be represented by a function, as follows:

$$f(x) = \frac{1}{\sqrt{\pi}\sigma}\int g(x - x_{th} + q)\exp(-\frac{q^2}{2\sigma^2})dq, \qquad (4)$$

$$g(t) = \begin{cases} a\sqrt{t} + b + ct + dt^2 + et^3 + ft^4 & \text{for } t > 0 \\ 0 & \text{otherwise} \end{cases} \qquad (5)$$

where x_{th} is the threshold energy for quasifree Λ production. The threshold behaviour and the gross features of the quasifree spectrum were represented by square-root and polynomial functions. They were smeared by a Gaussian resolution function of $\sigma \sim 3$ MeV (FIT-2).

All of the spectra applied to the fitting procedure were corrected for the following.

(a) The fraction estimated to be due to pion decays was subtracted from the proton gated spectrum. A corresponding correction was made to the pion-gated spectrum.

(b) The background in each spectrum was estimated from that in the region $E_x < -10$ MeV, where no (π^+, K^+) process should take place. We assumed that the background was flat (constant) over the spectra, since the number of spurious (π^+, K^+) events seen in the spectra is quite low.

The curves in Figs. 4 and 5 demonstrate the structure of the spectra in the cases of FIT-1 and FIT-2, respectively. Both cases reproduced similar spectra. We took the averages of the peak yields obtained in the two cases. The differences were included in the systematic errors.

B. Energy spectrum of NM-decay protons

The energy spectrum of NM-decay nucleons is affected by several nuclear effects. To estimate the energy distribution of the nucleons ejected from the hypernuclei, the effects of the Fermi motion and intranuclear cascade were studied using a Monte Carlo simulation. The simulation included three major parts: (i) *the initial NM-decay*, (ii) *the intranuclear cascade*, and (iii) *the evaporation process*. Details concerning the simulation are described in the Appendix.

(i) *The initial NM-decay*. We considered the transition $\Lambda N \rightarrow NN$ in the initial NM-decay. The momentum distributions of the initial ΛN in the hypernucleus determine those of the final NN. The initial momentum distributions were given by the wave functions of Λ and N, respectively. A point interaction in the $\Lambda N \rightarrow NN$ process was assumed.

(ii) *The intranuclear cascade*. The intranuclear cascade process was described by scatterings of the decay nucleons with nucleons in the residual nucleus. The interaction cross sections were determined by the mean-free path obtained from the imaginary part of the optical potential. We considered only s-wave scatterings. The scattered nucleons were trapped by the residual nucleus when they were below the Fermi surface and the nucleus was excited.

(iii) *The evaporation process*. Nucleon evaporations from the excited residual nucleus took place after the intranuclear cascade. The spectrum was assumed to be characterized by an exponential function of the nuclear temperature.

Fig. 6-a shows a simulated energy spectrum of protons from the $\Lambda p \rightarrow pn$ process in ${}^{12}_{\Lambda}C$. One can see that the spectrum is characterized by three major components. Protons from the evaporation process are characterized by the exponential shape in the low-energy region. Bumps with a peak at around 60 MeV and a peak at around 80 MeV correspond to protons from the s-shell and the p-shell, respectively. The probability of the second process, such as evaporation and collisions, is estimated to be about 20%. Fig. 6-b shows the energy distribution of protons related to the $\Lambda n \rightarrow nn$ process. The cut-off for the low-energy protons makes the contribution from the second process small.

It is also necessary to estimate the geometrical effects as follows. Since the present experiment has no tracking detector for the decay particles, the vertex point could not be determined precisely enough to make corrections for energy losses of the decay particles in the target material. Particles passing through the edge of the decay counter volume also distort the energy spectrum. We employed a Monte-Carlo calculation to determine the detector response and to estimate the detection efficiency for the decay particles, including the solid angle and the PI function efficiency.

Fig. 7 shows the proton-energy spectrum detected by the decay counter in the simulation for the $\Lambda p \rightarrow pn$ process (histogram) together with that measured for the ground-state region (plotted with closed circles). The measured E_p spectrum was corrected for pion contamination. The simulation reproduced the present experimental data quite well.

Here, although we approximated the transition $\Lambda N \rightarrow NN$ with a point interaction, it may depend upon the ΛN-spin configuration. As can be seen in Fig.6-a, the s-shell and p-shell nucleons gave different spectra. Changes in the s-shell component to the p-shell component affect the estimation of the solid angles. We considered two extreme cases. One is the case in which only the s-shell component contributed to the spectrum. The other is the case using only the p-shell component. The difference was taken into account as systematic errors on the solid angles.

We obtained the solid angles $\varepsilon_p\Omega_p = 23.2^{+0.9}_{-7.6}$ % and $\varepsilon_n\Omega_p = 0.8^{+0.9}_{-0.6}$ % for ${}^{12}_{\Lambda}C$, and, $\varepsilon_p\Omega_p = 22.2^{+0.4}_{-5.9}$ % and $\varepsilon_n\Omega_p = 0.7^{+0.9}_{-0.4}$ % for ${}^{11}_{\Lambda}B$, respectively, where the ε_p and the ε_n represent the efficiency for detected protons with $E_t > 45$ MeV in the $\Lambda p \rightarrow pn$ and $\Lambda n \rightarrow nn$ processes, respectively.

C. Branching Ratios and Weak-Decay Partial Rates

By definition, the branching ratios $R=\Gamma_n/\Gamma_p$, $b_p=\Gamma_p/\Gamma_{tot}$ and $b_{nm}=\Gamma_{nm}/\Gamma_{tot}$ satisfy the relationship

$$b_{nm} = (1+R)\times b_p. \tag{6}$$

Here, Γ_{tot} represents the total decay rate of a Λ hypernucleus. Quantities b_p and b_{nm} are branching ratios of the $\Lambda p \to pn$ process and the total NM-decay, respectively. The observed protons also include those which originate in the $\Lambda n \to nn$ process, since a proton may be kicked out of the nucleus in the intranuclear cascade process. Protons may also be observed when the M-decay pions are absorbed in the residual nuclei. In practice, we cannot distinguish the pion-absorbed M-decay from the NM-decays. It is, however, interesting to examine the fraction of NM-decay events which are caused by real pion absorption. Assuming that the pion-absorbed M-decays yielded a proton-energy spectrum close to that of the NM-decays, we obtained

$$b_p = \frac{Y_p}{Y_s}\times[(R\varepsilon_n+\varepsilon_p)\Omega_p]^{-1}, \tag{7}$$

where Y_s and Y_p denote the peak yields observed in the singles and proton-gated hypernuclear excitation-energy spectra, respectively. The quantity b_{nm} can be written as a branching ratio of the mesonic process (Γ_m/Γ_{tot}) as follows:

$$\begin{aligned} b_{nm} &= 1-\frac{\Gamma_m}{\Gamma_{tot}} \\ &= 1-(1+r_\pi)\frac{Y_{\pi^-}}{Y_s}\times[\varepsilon_{\pi^-}\Omega_{\pi^-}]^{-1}, \end{aligned} \tag{8}$$

where r_π is the ratio of π^0 decays to π^- decays (b_{π^0}/b_{π^-}). Quantity Y_{π^-} denotes the peak yield observed in the pion-gated hypernuclear excitation-energy spectrum. We estimated the detection efficiency and the solid angle for negative pions $(\varepsilon_{\pi^-}\Omega_{\pi^-})$ using a Monte-Carlo simulation; the results were $\varepsilon_{\pi^-}\Omega_{\pi^-}=0.21$ and $\varepsilon_{\pi^-}\Omega_{\pi^-}=0.34$ for $^{12}_{\Lambda}$C and $^{11}_{\Lambda}$B, respectively. They were obtained for pions with $E_t > 25$ MeV. No systematic errors, as seen in case of the NM-decay nucleons, were taken into account.

We obtained $b_{\pi^-}=0.09\pm0.04\pm0.01$ for $^{12}_{\Lambda}$C and $0.15\pm0.03\pm0.01$ for $^{11}_{\Lambda}$B, respectively, as shown in Table 1. The first and second errors stand for the statistical and systematic errors, respectively. We made use of data from previous studies of the π^0-mesonic decay rate in order to evaluate the quantities b_{nm}, b_p and R. The experimental measurements of the π^0 decay branching ratio (b_{π^0}) [19] are listed in Table 1. We thus obtained the quantities b_p, b_{nm}, and R from eqs. (6), (7), and (8), as shown in Table 2.

The total decay rates were measured as 1.25 ± 0.18 for $^{12}_{\Lambda}$C and 1.37 ± 0.16 for $^{11}_{\Lambda}$B in units of the decay rate of Λ hyperon in free space (Γ_Λ) by Grace *et al.* [7]. From these values and the obtained branching ratios, we derived the decay partial rates $(\Gamma_{\pi^-}$, Γ_p, and $\Gamma_{nm})$, as listed in Tables 3 and 4.

IV. DISCUSSIONS

A. M-decay rates

The present results for Γ_{π^-} are summarized in Table 3, and are compared with results

from other relevant studies. The BNL experiment reported $\Gamma_{\pi^-}=(0.052^{+0.063}_{-0.035})\Gamma_\Lambda$ in $^{12}_{\Lambda}$C [8]. This value does not contradict the present results concerning Γ_{π^-} in $^{12}_{\Lambda}$C. In the BNL experiment a large number of background events remained in the hypernuclear excitation-energy spectrum in the inclusive (K^-,π^-) reactions on ^{12}C. It possibly makes Γ_{π^-} small. They also reported an upper limit of $0.16\Gamma_\Lambda$ at the 95% confidence level. The present (π^+,K^+) experiment has kept the number of background events small in the excitation-energy spectrum. Montwill *et al.* have reported $Q^-=\Gamma_{nm}/\Gamma_{\pi^-}=4.8\pm1.1$ in $^{11}_{\Lambda}$B[20]. Here, we can extract a value for Γ_{π^-} of $(0.22\pm0.05)\Gamma_\Lambda$ from the following equations:

$$\Gamma_{\pi^0}/\Gamma_{\pi^-} = 0.5, \tag{9}$$

$$\Gamma_{tot} = \Gamma_{nm}+\Gamma_{\pi^-}+\Gamma_{\pi^0}, \tag{10}$$

as assumed in ref.[19]. Eq.(9) is required due to the empirical $\Delta I=1/2$ rule. The assumption is reasonable since no significant difference of the shell structure between the daughter nuclei in the π^- and π^0 decays of $^{11}_{\Lambda}$B affects the ratio. We can also extract a value for Γ_{π^-} of $(0.20\pm0.04)\Gamma_\Lambda$ using the ratio $\Gamma_{\pi^0}/\Gamma_{\pi^-}=r_\pi$ obtained from the present b_{π^-} and the previous b_{π^0} [19]. The present measurement of Γ_{π^-} in $^{11}_{\Lambda}$B agrees well with both extracted values.

It has been suggested that the suppression of M-decay is weakened, even in heavy hypernuclei, because the pion wave distortion and nucleon correlation in the nuclear medium make the decay probability large [1, 2]. Motoba *et al.* have studied the effects of pion distortion on p-shell hypernuclei by employing three different potentials, as shown in Table 3 [21]. FREE means no distortion. The MSU potential gave a larger distortion, and thus a larger Γ_π than that given by WHIS. The present result concerning Γ_{π^-} in $^{12}_{\Lambda}$C is close to that given by WHIS, although it does not contradict the others within errors. Γ_{π^-} in $^{11}_{\Lambda}$B is sensitive to the potential. The present Γ_{π^-} in $^{11}_{\Lambda}$B agrees well with that given by WHIS. The ratio of Γ_{π^-} in $^{12}_{\Lambda}$C to that in $^{11}_{\Lambda}$B is found to be $0.52\pm0.27\pm0.05$ in the present experiment. This value agrees with the calculations which are almost independent of the potentials. The present results show the effect of pion wave distortion on the M-decay rate.

B. NM-decay rates

The obtained $\Gamma_{nm}/\Gamma_\Lambda$ and Γ_n/Γ_p are displayed in Table 4 together with previous measurements and theoretical calculations. We can extract $\Gamma_{nm}=(1.06\pm0.34)\Gamma_\Lambda$ in $^{11}_{\Lambda}$B from the Q^- given by Montwill *et al.* [20] employing eqs.(9) and (10). The present results concerning Γ_{nm} show almost unity in units of Γ_Λ, and agree well with the previous measurements. The BNL experiment measured neutrons and protons stimulated from the hypernuclei [8]. The large errors are due to low efficiencies and large backgrounds in neutron detection. The present experiment found that Γ_n is almost twice the size of Γ_p in both $^{12}_{\Lambda}$C and $^{11}_{\Lambda}$B, although the results have sizable errors. Mangotra *et al.* [22] and Montwill *et al.* [20] reported $\Gamma_n/\Gamma_p=2.11^{+0.36}_{-0.29}$ and $0.59^{+0.17}_{-0.14}$, respectively. Both emulsion experiments failed to identify the hypernuclear isotope.

Dubach *et al.* have calculated the NM-decay rates in nuclear matter based on meson-exchange models, and assumed a relative s wave in the initial ΛN system [4]. Their one pion exchange calculation gave a large Γ_{nm} of 2∼4 and a very small Γ_n, where the tensor term was strongly enhanced and the neutron-induced transition was forbidden. It is reasonable to take the short-range effects into account since the $\Lambda N \to NN$ transition involves a large momentum transfer of ~ 400 MeV/c. Dubach *et al.* also studied heavier meson effects in the calculation. Considering π, ρ, η, ω, K, and K^*, they obtained Γ_{nm}=1.23Γ_Λ and Γ_n/Γ_p=0.34, which improved the calculated values, but still suppressed Γ_n. Cheung, Heddle, and Kisslinger calculated Γ_{nm} by employing the quark hybrid model, where the 6-quark state was taken into account in the short-range region. They obtained Γ_{nm}=1.28Γ_Λ in $^{12}_\Lambda$C using the ΔI=1/2 rule [23]. The value is consistent with the measured Γ_{nm}. Ramos *et al.* calculated the NM-decay rates in finite hypernuclei, $^5_\Lambda$He, $^{11}_\Lambda$B, and $^{12}_\Lambda$C, based on a one-pion exchange model with a relativistic nuclear treatment [24]. The authors have pointed out that the contribution of a p-shell nucleon is of importance to the decay amplitudes. The calculation gave the parity-violating and parity-conserving amplitudes, and reproduced the asymmetry of protons in the NM-decay from polarized hypernuclei. This has been reported elsewhere [10]. They have reported Γ_{nm}=0.98Γ_Λ and Γ_n/Γ_p=0.27 for π, ρ, η, ω, K, and K^* meson exchanges in $^{12}_\Lambda$C [5]. Although the Γ_{nm} is in good agreement with the measured values, the Γ_n/Γ_p is still quite different from the measured values.

Ericson *et al.* have suggested that multinucleon-induced processes, such as $\Lambda NN \to NNN$, play an important role in NM-decay [6]. The process is caused by the absorption of a virtual (off-shell) pion from a decaying Λ into a pair of nucleons or more. It reflects the propagation of the pion through the nuclear medium, which is strongly related to the M-decay process. They found that the processes contributed to 30~40% of the total NM-decay rate. The two-body NM-decay rate is then written as

$$\Gamma^{(2)}_{nm} = (0.6 \sim 0.7) \times \Gamma_{nm} \tag{11}$$

$$\equiv \Gamma^{(2)}_p + \Gamma^{(2)}_n, \tag{12}$$

where superscript (*2*) means two-body NM-decay. This may explain the discrepancy in Γ_n/Γ_p. Multinucleon-induced decay would feed the low-energy region in the proton-energy spectrum because the released energy is shared by 3 particles or more. Unfortunately, our detectors had poor sensitivity to protons with E_p below ~40 MeV, due mainly to the thickness of the target and the ΔE counter. If we were completely insensitive to this component, our result for Γ_p could represent the two-body NM-p decay rate ($\Gamma^{(2)}_p$) and, hence, $\Gamma^{(2)}_n/\Gamma^{(2)}_p$ would be 40~70% smaller than our results for Γ_n/Γ_p.

The structure of the nucleon-energy spectrum may be sensitive to the detailed mechanism involved in hypernuclear NM-decays. In particular, the structure of the low-energy region is useful for studying the multinucleon process. A precise measurement of low-energy protons, and also neutrons if possible, from the NM-decay is required to study the problem further.

V. CONCLUSIONS

In the present study we measured the M-decay and NM-decay rates, which are key observables for studying weak decays. The measured Γ_{π^-} shows that Pauli blocking is less effective due to pion distortion than expected in $^{12}_\Lambda$C and $^{11}_\Lambda$B. The previous Γ_{π^0} measurement in $^{12}_\Lambda$C and $^{11}_\Lambda$B also suggested a strong distortion effect, although it was much stronger than that predicted by a calculation [19, 21]. Both experiments demonstrate

that pion distortion in the nuclear medium plays an important role in the suppression of hypernuclear mesonic decay. Systematic measurements with a mass number dependence are necessary for a further understanding of M-decays.

The present result concerning Γ_{nm} is consistent with previous measurements and in good agreement with the theoretical calculations. The present measurement shows that Γ_n is almost twice the size of Γ_p, although the obtained Γ_n/Γ_p ratios in $^{12}_\Lambda$C and $^{11}_\Lambda$B have sizable errors. The previous measurements gave a ratio of almost unity, while the calculations suggested a more strongly suppressed Γ_n. There are still discrepancies between the experimental values and the theoretical calculations. The multinucleon-induced process in NM-decay may account for this discrepancy. Precise studies on the structure of the nucleon-energy spectrum, particularly in low-energy region, are needed to examine the multinucleon process in NM-decays.

ACKNOWLEDGEMENT

The authors thank Professors H. Sugawara, K. Nakai, K. Takamatsu, M. Takasaki, T. Sato, J. Chiba, T. K. Ohska, M. Kihara and the crew of the KEK PS for their support and encouragement to carry out the experiment. They are grateful to the collaborators of the present E160 experiment.

APPENDIX

A. Monte-Carlo simulation

We considered a phenomenological model for the NM-decay process to estimate the energy distribution of stimulated nucleons. The process includes three major parts: (i) *the initial NM-decay*, (ii) *the intranuclear cascade*, and (iii) *the evaporation process*, as mentioned in section III-B.

We can describe the momentum distribution of the two nucleons in the final channel of the NM-decay as follows:

$$\frac{d^6 D(\boldsymbol{p}_1, \boldsymbol{p}_2)}{d\boldsymbol{p}_1 d\boldsymbol{p}_2} = |< N_1\boldsymbol{p}_1 N_2\boldsymbol{p}_2; A\text{-}2|V_{\Lambda N}|^A_\Lambda Z >|^2, \tag{13}$$

where $|^A_\Lambda Z>$ represents the initial hypernuclear state; the final state is expressed by the two-nucleon state of N_1 and N_2 with momenta of $\boldsymbol{p}_1$ and $\boldsymbol{p}_1$ and the residual nuclear state of mass number A-2. Quantity $V_{\Lambda N}$ stands for the potential driving the $\Lambda N \to NN$ transition. The $V_{\Lambda N}$ interaction is characterized by short-range effects, since the $\Lambda N \to NN$ transition involves a large momentum transfer of ~400 MeV/c. We approximated $V_{\Lambda N}$ by a point interaction. We considered the plane waves of the final two nucleons and solved eq.(13) as

$$\frac{d^6 D(\boldsymbol{p}_1, \boldsymbol{p}_2)}{d\boldsymbol{p}_1 d\boldsymbol{p}_2} = \sum_\alpha \int d\boldsymbol{k}_\Lambda |\phi^\Lambda(\boldsymbol{k}_\Lambda)|^2 \int d\boldsymbol{k}_N |\phi^N_\alpha(\boldsymbol{k}_N)|^2 \delta(p_1 + p_2 - p_\Lambda - p_N). \tag{14}$$

Here, we required both energy and momentum conservation in the $\Lambda N \to NN$transition. The p_Λ=(E_Λ, $\boldsymbol{k}_\Lambda$), p_N=(E_N, $\boldsymbol{k}_N$), p_1=(E_1, $\boldsymbol{p}_1$), and p_2=(E_2, $\boldsymbol{p}_2$) denote the four-momenta of the initial Λ and N, and the final two nucleons, respectively. Since the initial Λ is bound, the total energy (E_Λ) is described as

$$E_\Lambda = m_\Lambda - B_\Lambda - \frac{|\boldsymbol{k}_\Lambda|^2}{2M_R}, \tag{15}$$

where B_Λ stands for the Λ-separation (Λ-binding) energy; m_Λ and M_R are the masses of the Λ and the residual nucleus. The momentum distributions of the Λ and N were given by the momentum-space wave functions, $\phi^\Lambda(\boldsymbol{k}_\Lambda)$ and $\phi_\alpha^N(\boldsymbol{k}_N)$, in the initial state. Subscript α represents the shell (orbital) of the nucleon. We assumed that Λ lies in the s-orbital before the NM-decay.

The decay nucleons may be scattered by the nucleons in the residual nucleus, since they have finite mean-free paths. We consider the factor G, which represents a fraction of the missing flux due to scattering. The factor G depends upon the position $\boldsymbol{r}$ in the nucleus and the momentum of the decay nucleon, as described below:

$$G_\alpha(\boldsymbol{r},\boldsymbol{p}) = \int \rho_\alpha^{\Lambda N}(\boldsymbol{r}) \exp[-\hat{T}(\boldsymbol{r},\boldsymbol{e};\boldsymbol{p})] d\Omega_{\boldsymbol{e}}, \tag{16}$$

where $\rho_\alpha^{\Lambda N}(\boldsymbol{r})$ denotes the density distribution of the ΛN, which can be expressed as

$$\rho_\alpha^{\Lambda N}(\boldsymbol{r}) = \int d(\boldsymbol{r}')|\psi^\Lambda(\boldsymbol{r})\psi_\alpha^N(\boldsymbol{r}')|^2\delta(\boldsymbol{r} - \boldsymbol{r}'). \tag{17}$$

Here, ψ^Λ and ψ_α^N are the coordinate representations of the Λ and N wave functions. $\hat{T}$ stands for the thickness of the nucleus measured in units of the mean-free path ($\lambda(\boldsymbol{p})$), and seen from position $\boldsymbol{r}$ in the direction $\boldsymbol{e}$. It is expressed as

$$\hat{T}(\boldsymbol{r},\boldsymbol{e};\boldsymbol{p}) = \int \frac{dz}{\lambda(\boldsymbol{p})} \cdot \frac{\rho_N(\boldsymbol{r}+z\boldsymbol{e})}{\rho_N(0)}, \tag{18}$$

where ρ_N represents the nucleon-density distribution of the residual nucleus.

In practice, it is complicated to unify the initial NM-decay with the intranuclear cascade process. A method to do this can be found in a study by Chiang and Hüfner [25]. We employed a Monte-Carlo simulation. In the simulation the initial NM-decay took place according to eq.(14). The decay nucleons were then allowed to scatter until they were emitted or trapped by the nucleus. An NM-decay point was given by eq.(17) and the scattering point was evaluated from eq.(18). We calculated single-particle wave functions for the ϕ's and ψ's, as described in next subsection. The mean-free path was estimated from the imaginary part of the optical potential [26]. We then considered s-wave scatterings in the initial NM-decay and the intranuclear cascade. The scattered nucleons cannot escape from the nucleus when their total energies in the two body center-of-mass frame are below the nucleon mass (they would be below the Fermi surface). They were consequently trapped by the nucleus and excited the nucleus.

Nucleon evaporations from the excited residual nucleus took place after the intranuclear cascade. The spectrum was assumed to be characterized by an exponential function of the nuclear temperature.

When a Λ hyperon is polarized by the (π^+, K^+) reaction at a finite scattering angle, NM-decay protons have an asymmetric angular distribution of $W(\theta) \sim 1 + P_\Lambda A_1 \cos\theta$, where P_Λ and A_1 represent the Λ-spin polarization and the asymmetry parameter, respectively [27, 28]. The second term introduces a so-called up-down asymmetry with respect to the reaction plane defined by $\boldsymbol{k}_{\pi^+} \times \boldsymbol{k}_{K^+}$. A measurement of the asymmetry for the NM-decay protons is another interesting subject, and a goal of the PS E160 experiment. This has already been reported elsewhere [10]. The nuclear effects modify the angular distribution and attenuates the asymmetry. We also evaluated the attenuation factor by means of the simulation code.

B. Wave functions

We used the Wood-Saxon potential to obtain single-particle wave functions of the hyperon and nucleons. It is described as

$$V(r) = V_0 f(r) + V_{so}\left(\frac{\hbar}{m_\pi c}\right)^2 \frac{1}{r}\frac{\mathrm{d}f}{\mathrm{d}r}(\boldsymbol{\ell}\cdot\boldsymbol{\sigma}) + V_C, \tag{19}$$

where

$$f(r) = \left[1 + \exp(\frac{r-c}{a})\right]^{-1}. \tag{20}$$

Here, V_C represents the Coulomb potential assuming a uniform charge distribution inside the nuclear radius (c). Parameters relevant to the potential are summarized in Table 5. We used hypernuclear radii $c = < r^2 >^{1/2}$ parametrized by the analysis in ref. [29]. The V_0's were adjusted so as to reproduce the given separation energy, for which the binding energy in the $p_{3/2}$-nucleon [30] and $s_{1/2}$-Λ [31] were used. The V_{so}'s were assumed to be 5 MeV for the nucleons, and negligible for the hyperon [32, 33, 34]. The binding energies of $s_{1/2}$-nucleons were obtained by the given potential. Fig. 8 displays the radial wave functions obtained for the s-shell hyperon (solid line), the s-shell proton (dashed line), and the p-shell proton (dotted line) in ${}^{12}_{\Lambda}$C. The momentum distribution of the hyperon and nucleons in the hypernuclei are also displayed in the same figure.

References

[1] H. Bandō and H. Takaki, Prog. Theor. Phys., **72**, 106(1984); Phys. Lett. **150B**, 409(1985); H. Bandō, Prog. Theor. Phys. Suppl. **81**, 181(1985).

[2] E. Oset and L. L. Salcedo, Nucl. Phys. **A443**, 704(1985).

[3] K. Takeuchi, H. Takaki and H. Bandō, Prog. Theor. Phys. **73**, 841(1985).

[4] J. F. Dubach, Nucl. Phys. **A450**, 71c(1986).

[5] A. Ramos and C. Bennhold, Nucl. Phys. **A577**, 287c(1994).

[6] M. Ericson, Nucl. Phys. **A547**, 127c(1992); W. M. Alberico, A. De Pace, M. Ericson and A. Molinari, Phys. Lett. **B256**, 134(1991).

[7] R. Grace *et al.*, Phys. Rev. Lett. **55**, 1055(1985).

[8] J. J. Szymanski *et al.*, Phys. Rev. **C43**, 849(1991).

[9] H. Ejiri *et al.*, KEK Proposal E160, OULNS **89-1**, (1989).

[10] S. Ajimura *et al.*, Phys. Lett. **B282**, 293(1992); S. Ajimura *et al.*, Phys. Rev. Lett. **68**, 2137(1992).

[11] A. Yamamoto *et al.*, KEK Report **81-13**,(1981).

[12] M. Akei *et al.*, Nucl. Instrum. Methods Phys. Res., Sect. **A283**, 46(1989); M. Akei *et al.*, Nucl. Phys. **A534**, 478(1991).

[13] L. Lee *et al.*, Nucl. Instrum. Methods Phys. Res. **A372**, 287(1993).

[14] T. Motoba, H. Bandō, R. Wünsch, and J. Žofka, Phys. Rev. **C38**, 1322(1988).

[15] T. Hasegawa *et al.*, Phys. Rev. Lett., **74**, 224(1995).

[16] M. Juric *et al.*, Nucl. Phys. **B47**, 36(1972); W. Bruckner *et al.*, Phys. Lett. **B55**, 107(1975); R. Bertini *et al.*, Nucl. Phys. **A360**, 315(1981); R. E. Chrien *et al.*, Phys. Lett. **B89**, 31(1979); C. Milner *et al.*, Phys. Rev. Lett. **54**, 1237(1985).; R. Chrien, AIP conference proceedings No. 224, Particle and field series 43, 1990, p.28

[17] K. Itonaga *et al.*, Proc. 5th Int. Symp. Mesons and Light Nuclei, Prague (1991), and private communication.

[18] T. Kishimoto *et al.*, Phys. Rev. Lett., in press.

[19] A. Sakaguchi *et al.*, Phys. Rev. **C43**, 73(1991).

[20] A. Montwill *et al.*, Nucl. Phys. **A234**, 413(1974).

[21] T. Motoba, K. Itonaga and H. Bandō, Nucl. Phys. **A489**, 683(1988).

[22] L. K. Mangotra *et al.*, Nuovo Cimento **13A**, 826(1973).

[23] C. -Y. Cheung, D. P. Heddle and L. S. Kisslinger, Phys. Rev. C27, 335(1983); D. P. Heddle and L. S. Kisslinger, *ibid.* **C33**, 608(1986).

[24] A. Ramos, C. Bennhold, E. van Meijgaard and B. K. Jennings, Nucl. Phys. **A554**, 703(1992); A. Ramos, C. Bennhold, E. van Meijgaard and B. K. Jennings, Phys. Lett. **B264**, 233(1991).

[25] H. C. Chiang and J. Hüfner, Nucl. Phys. **A352**, 442(1981).

[26] J. J. H. Menet, E. E. Gross, J. J. Malanify, and A. Zucker, Phys. Rev. C4, 1114(1971).

[27] H. Ejiri, T. Fukuda, T. Shibata, H. Bandō, and K.-I. Kubo, Phys. Rev. **C36**, 1435(1987).

[28] H. Bandō, T. Motoba, M. Sotona, and J. Žofka, Phys. Rev. **C39**, 587(1989).

[29] D. J. Millener, C. B. Dover and A. Gal, Phys. Rev. **C38**, 2700(1991).

[30] F. Ajzenberg-Selove, Nucl. Phys. **A490**, 1(1988).; F. Ajzenberg-Selove, *ibid* **A506**, 1(1990).

[31] M. Juric *et al.*, Nucl. Phys. **B52**, 1(1973);

[32] W. Bruckner *et al.*, Phys. Lett. **B79**, 157(1978).

[33] H. Piekarz *et al.*, Phys. Rev. Lett. **47**, 1106(1981).

[34] E. H. Auerbach *et al.*, Phys. Rev. Lett. **47**, 1110(1981).

Table Captions

Table 1 Branching ratios for mesonic π^- decay (b_{π^-}). The first and second errors appearing in the results stand for the statistical and systematic errors, respectively. Other experimental results concerning mesonic π^0 decay (b_{π^0}) and theoretical calculations concerning the ratios (r_π) of π^0 decay to π^- decay are listed for reference.

Table 2 Branching ratios for NM-proton decay (b_p), total NM-decay (b_{nm}), and ratios (R) of NM-neutron decay to NM-proton decay. The first and second errors appearing in all of the entries indicate the statistical and systematic errors, respectively.

Table 3 Present results for Γ_{π^-}. The previous measurements and calculations are listed for a comparison. Allof the entries are in units of the free Λ decay width (Γ_Λ), but for ratios of Γ_{π^-} in ${}^{12}_{\Lambda}$C to that in ${}^{11}_{\Lambda}$B.

Table 4 Present results for Γ_p, Γ_{nm}, and Γ_n/Γ_p. The previous measurements and calculations in p-shell hypernuclei are listed for reference. All of the entries are in units of the free Λ decay width (Γ_Λ), but for Γ_n/Γ_p's.

Table 5 Wood-Saxon potential parameters used for calculating the wave functions. B.E. denotes the binding energy of Λ and N. Quantities a and c represent the diffusivity and radius of the potential, respectively. V_0 and V_{so} are the potential depth corresponding to the leading and spin-orbit forces, respectively.

Figure Captions

Fig. 1 Schematic view of the experimental setup. Counter telescopes for decay particles from hypernuclei were newly installed in the PIK spectrometer constructed for the previous experiment [12]. The pion beam was defined by counter hodoscopes BH1 and BH2. Positrons contaminated in the beam were rejected by a gas Čerenkov counter GČ. The momenta of the pions were analyzed by the magnetic spectrometer (PIK-BA) and drift chambers (BDC1∼5). Differential lucite Čerenkov counters (BLČ's) were located behind an active scintillator target (TGT) to discard beam pions passing through, but not interacting with, the target. Scattered particles were triggered by a hodoscope TOF. Kaons were discriminated by two Čerenkov detectors, LČ and AČ. The momenta of the kaons were reconstructed by the magnetic spectrometer (PIK-PA) and drift chambers (SDC1∼4). The decay counter telescopes were set above and below the target. Each counter telescope set comprised an array of ΔE (plastic) and E (NaI) counters.

Fig. 2 Scattered particle masses reconstructed from the measured momentum and time-of-flight between BH2 and TOF. The kaons are clearly separated from other particles. The proton mass is slightly shifted because the velocity-reconstruction function from the time-of-flight is optimized for kaons.

Fig. 3 Typical PI spectrum for decay particles whose energy is higher than 25 MeV. The vertical solid and dashed lines define the windows of gating pions and protons, respectively.

Fig. 4 (π^+, K^+) singles spectrum (a), and spectra gated by the decay protons (b) and by the decay pions (c). The curves indicate the structure of the spectra obtained by the fitting procedure *FIT*-1. In *FIT*-1, two Gaussian peaks of $\sigma \sim 3$ MeV at $E_x = 0$ MeV (1^-) and $E_x = 10$ MeV (2^+) and the calculated states from ref. [17] in the Λ-unbound (Λ-UB) region ($E_x > 11$ MeV) were assumed. Contamination (C) of pions in the proton-gated spectrum because of the impurity in the PI window for protons was corrected. A corresponding correction was made to the pion-gated spectrum, and pion-gated spectra. The background (BG) estimated from that in the $E_x < -10$ MeV region was subtracted from each spectrum.

Fig. 5 Same as Fig. 4, but the fitting procedure *FIT*-2 was used to reproduce the spectra.

Fig. 6 Proton-energy (E_p) spectrum from the $\Lambda p \to pn$ process in ${}^{12}_{\Lambda}$C obtained by a Monte-Carlo simulation (a). Three major components (protons from the evaporation process, those from the s-shell, and those from the p-shell) are shown. The simulated proton-energy spectrum from the $\Lambda n \to nn$ process in ${}^{12}_{\Lambda}$C is shown in (b).

Fig. 7 Proton-energy (E_p) spectrum observed in the ground-state region (circles with error bars). The histogram was obtained by a simulation, in which the geometry of the decay counter telescopes and the energy loss effect in the materials were considered. The energy distribution of the protons obtained by the intranuclear cascade calculation were used as an input of the simulation.

Fig. 8 Density distributions of the radial wave functions obtained for the s-shell hyperon, the s-shell proton, and the p-shell proton in ${}^{12}_{\Lambda}$C (upper). The momentum distributions of the Λ and N were given by the momentum-space wave functions (lower).

	Experiment		Theory [21]		
	b_{π^-} present	b_{π^0} Sakaguchi [19]	Free	Γ_π MSU	WHIS
${}^{12}_{\Lambda}$C	$0.09 \pm 0.04 \pm 0.01$	$0.174 \pm 0.057 \pm 0.008$	1.35	1.26	1.18
${}^{11}_{\Lambda}$B	$0.15 \pm 0.03 \pm 0.01$	$0.140 \pm 0.039 \pm 0.025$	0.47	0.48	0.47

Table 1:

${}^{A}_{\Lambda}Z$	b_p	b_{nm}	R
${}^{12}_{\Lambda}$C	$0.27 \pm 0.04^{+0.09}_{-0.02}$	$0.74 \pm 0.08 \pm 0.01$	$1.74 \pm 0.51^{+0.23}_{-0.94}$
${}^{11}_{\Lambda}$B	$0.24 \pm 0.04^{+0.07}_{-0.03}$	$0.77 \pm 0.05 \pm 0.03$	$2.25 \pm 0.57^{+0.39}_{-0.94}$

Table 2:

	Experiment			Theory [21]		
	present	BNL [8]	Montwill [20]	FREE	WHIS	MSU
$\Gamma_{\pi^-}({}^{12}_{\Lambda}\mathrm{C})/\Gamma_\Lambda$	$0.11 \pm 0.05 \pm 0.01$	$0.052^{+0.063}_{-0.035}$		0.058	0.107	0.134
$\Gamma_{\pi^-}({}^{11}_{\Lambda}\mathrm{B})/\Gamma_\Lambda$	$0.21 \pm 0.05 \pm 0.01$		0.22 ± 0.05	0.134	0.223	0.294
$\Gamma_{\pi^-}({}^{12}_{\Lambda}\mathrm{C})/\Gamma_{\pi^-}({}^{11}_{\Lambda}\mathrm{B})$	$0.52 \pm 0.27 \pm 0.05$			0.433	0.480	0.456

Table 3:

${}^{A}_{\Lambda}Z$	Γ_p/Γ_Λ	$\Gamma_{nm}/\Gamma_\Lambda$	Γ_n/Γ_p	refs.
Experiment				
${}^{12}_{\Lambda}C$	$0.34 \pm 0.07^{+0.11}_{-0.03}$	$0.93 \pm 0.17 \pm 0.01$	$1.74 \pm 0.54^{+0.23}_{-0.94}$	present
${}^{11}_{\Lambda}B$	$0.33 \pm 0.07^{+0.10}_{-0.04}$	$1.05 \pm 0.14 \pm 0.04$	$2.25 \pm 0.57^{+0.39}_{-0.94}$	present
$A > 10$			$2.11^{+0.36}_{-0.29}$	[22]
${}_{\Lambda}B, {}_{\Lambda}C, {}_{\Lambda}N$			$0.59^{+0.17}_{-0.14}$	[20]
${}^{12}_{\Lambda}C$		1.14 ± 0.20	$1.33^{+1.12}_{-0.81}$	[8]
${}^{11}_{\Lambda}B$			$1.04^{+0.59}_{-0.48}$	[8]
Theory				
$A = \infty$		1.23	0.34	[4]
${}^{12}_{\Lambda}C$		1.28		[23]
${}^{12}_{\Lambda}C$		0.98	0.27	[5]

Table 4:

		B.E.$(s_{\frac{1}{2}})$ (MeV)	B.E.$(p_{\frac{3}{2}})$ (MeV)	a (fm)	c (fm)	V_0 (MeV)	V_{so} (MeV)
${}^{12}_{\Lambda}C$	Λ	10.8	–	0.54	2.79	25.5	–
${}^{11}C$	p	24.8	8.69	0.54	2.52	54.8	5.0
	n	30.3	13.1	0.54	2.52	57.2	5.0
${}^{11}_{\Lambda}B$	Λ	10.2	–	0.54	2.72	25.3	–
${}^{10}B$	p	21.5	6.59	0.54	2.49	46.1	5.0
	n	24.1	8.44	0.54	2.49	49.7	5.0

Table 5:

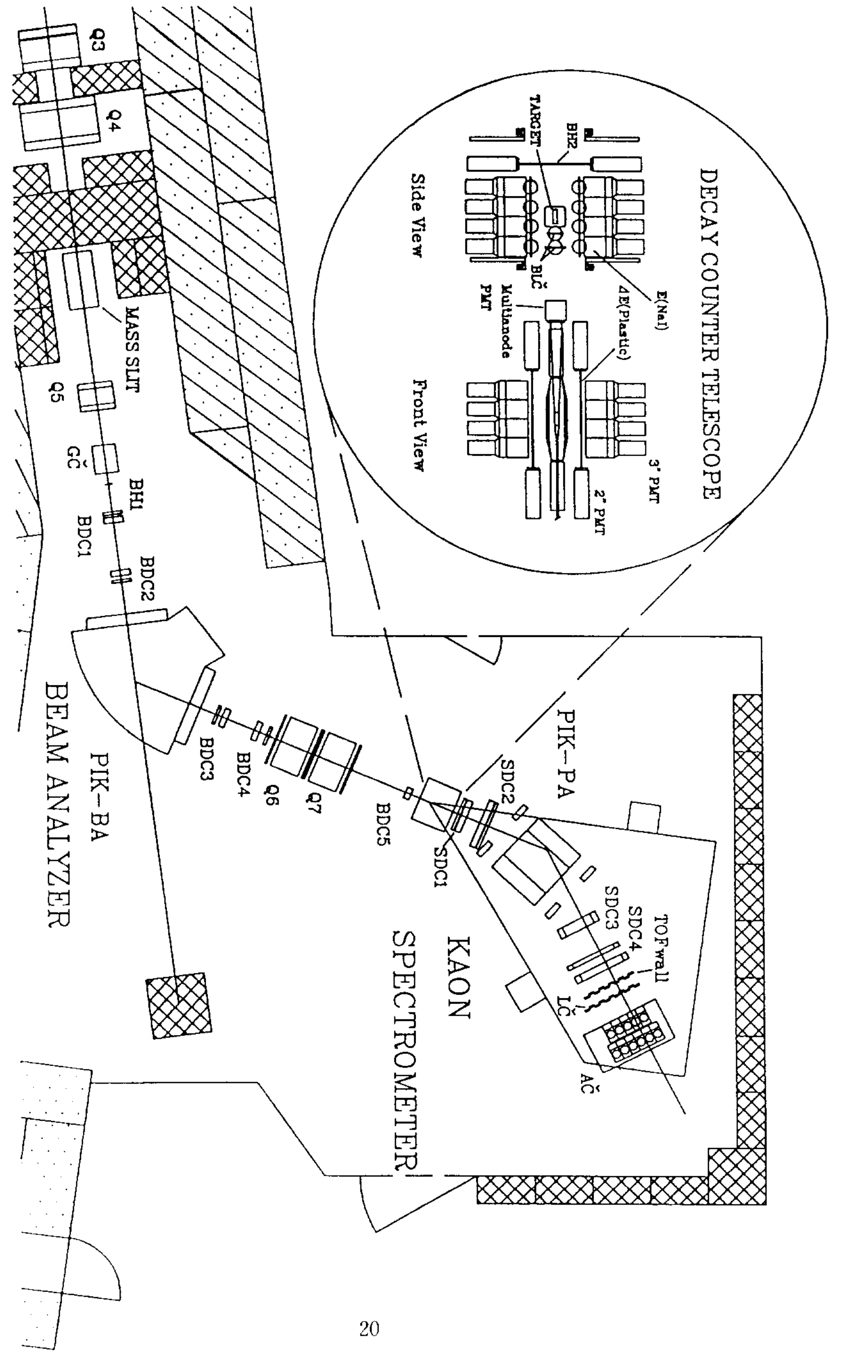

Fig. 1

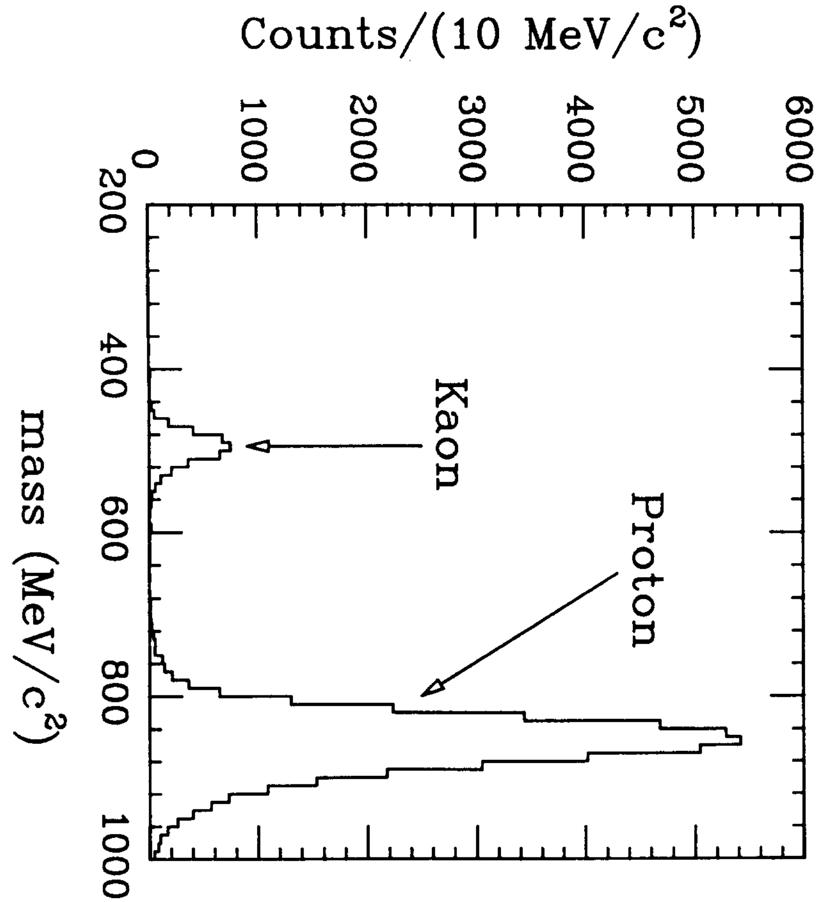

Counts/(10 MeV/c²)
mass (MeV/c²)
Kaon
Proton

Fig. 2

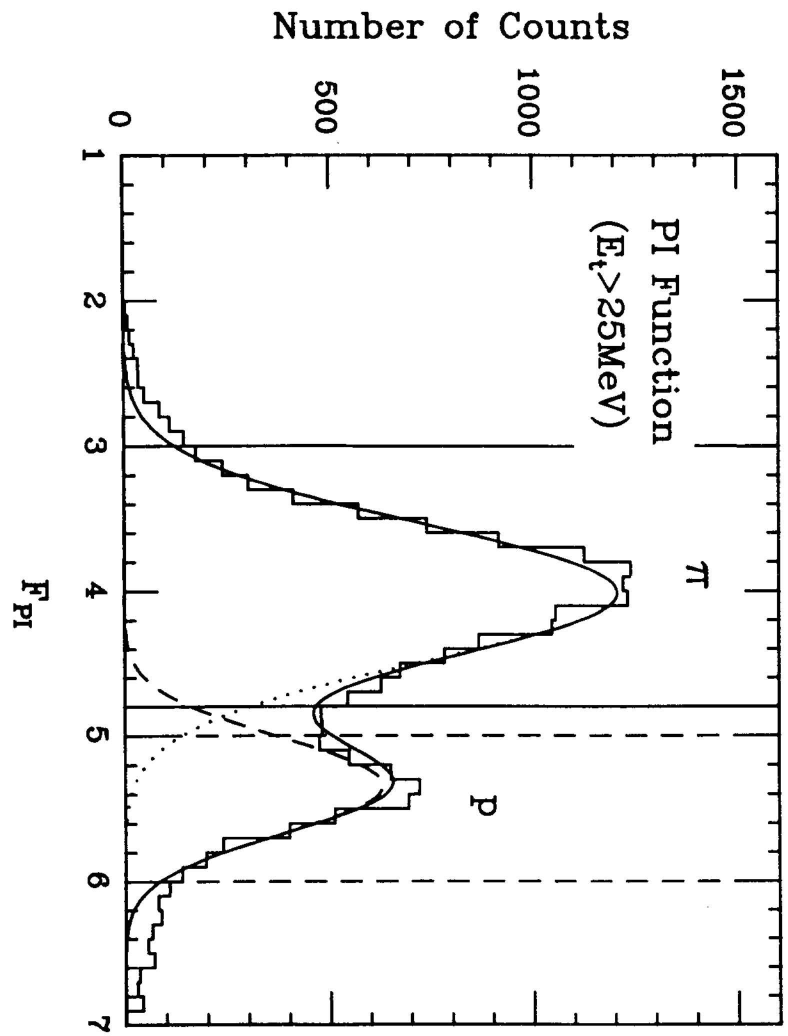

Number of Counts
PI Function
(Et>25MeV)
π
p
FPI

Fig. 3

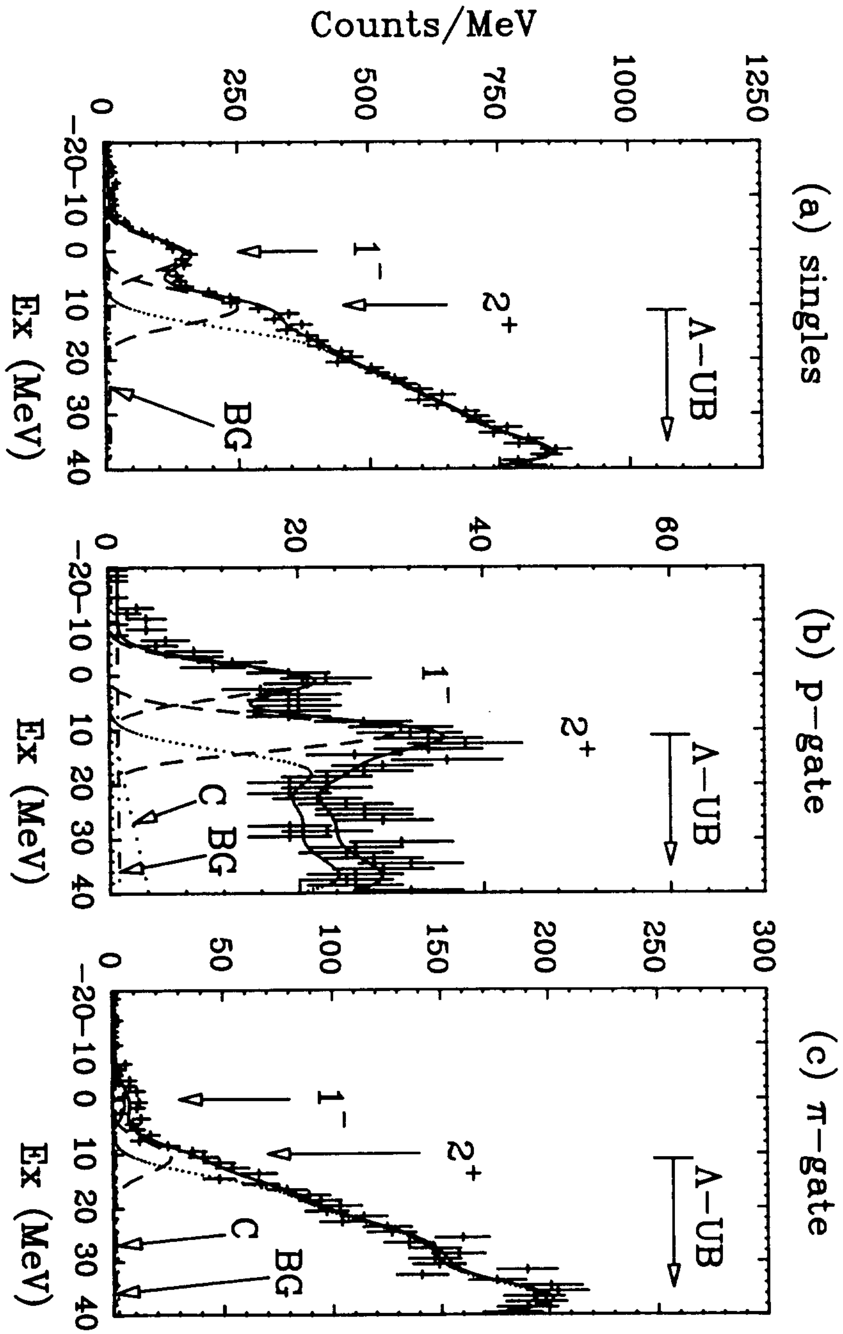

Counts/MeV
(a) singles
(b) p−gate
(c) π−gate
Λ−UB
1⁻
2⁺
C
BG
Ex (MeV)

Fig. 4

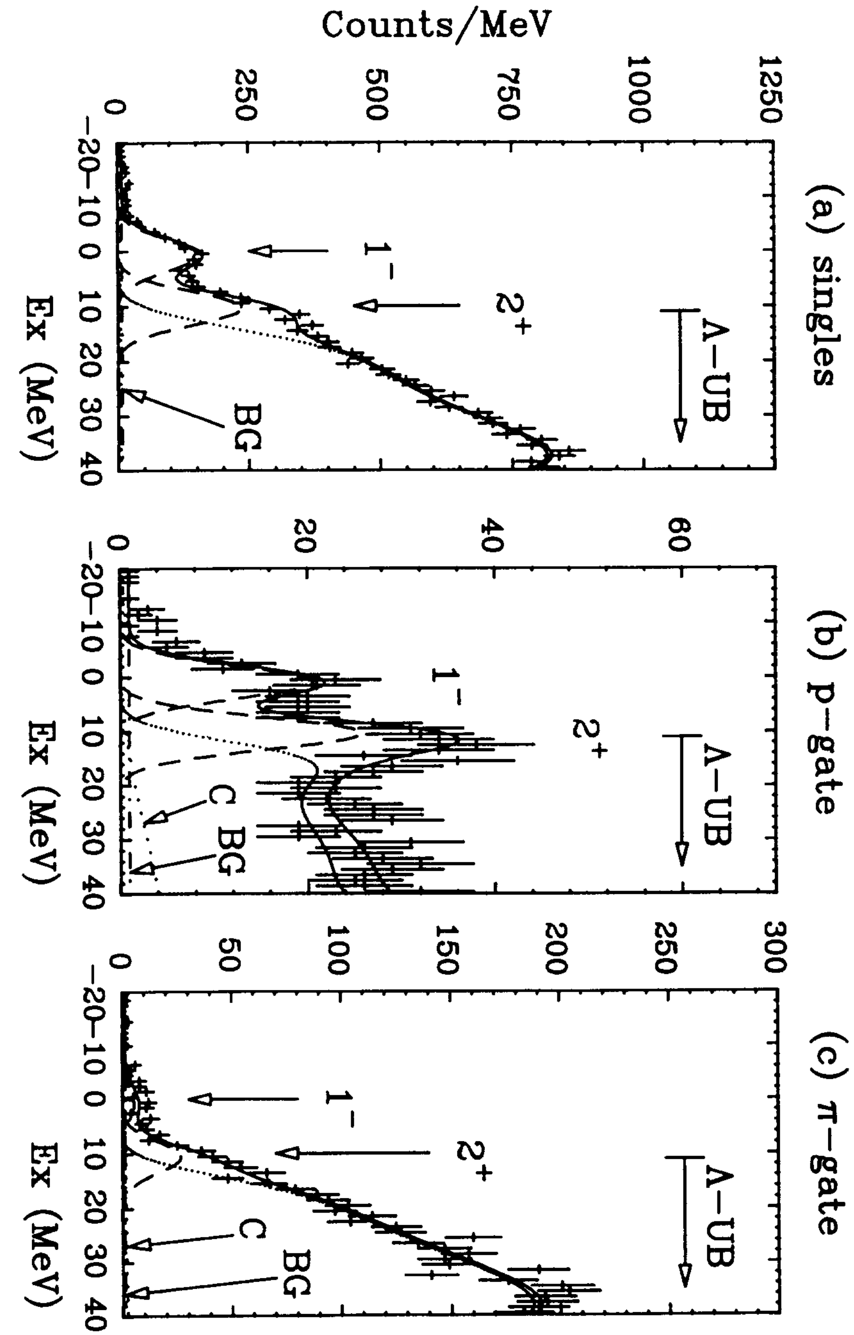

Counts/MeV
(a) singles
(b) p−gate
(c) π−gate
Λ−UB
1⁻
2⁺
C
BG
Ex (MeV)

Fig. 5

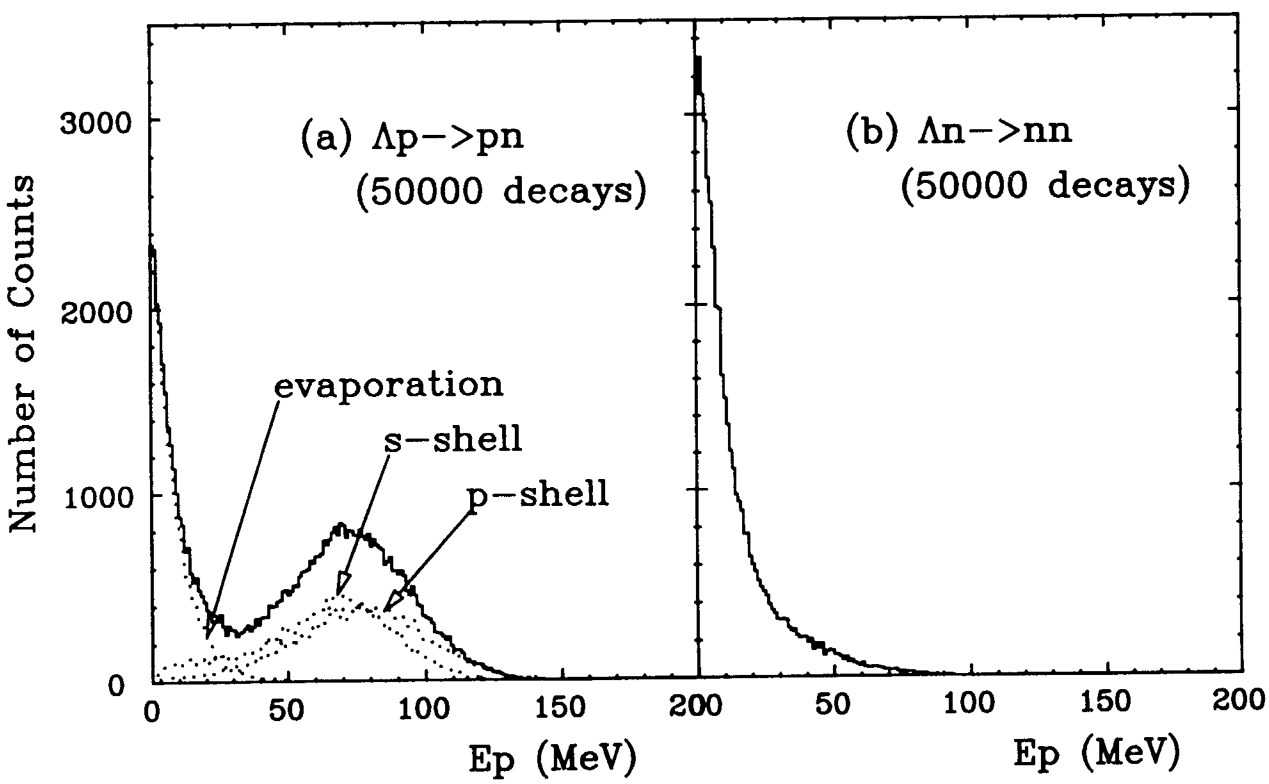

Number of Counts
0
1000
2000
3000
(a) Λp−>pn
(50000 decays)
evaporation
s−shell
p−shell
(b) Λn−>nn
(50000 decays)
0
50
100
150
200
50
100
150
200
Ep (MeV)
Ep (MeV)

Fig. 6

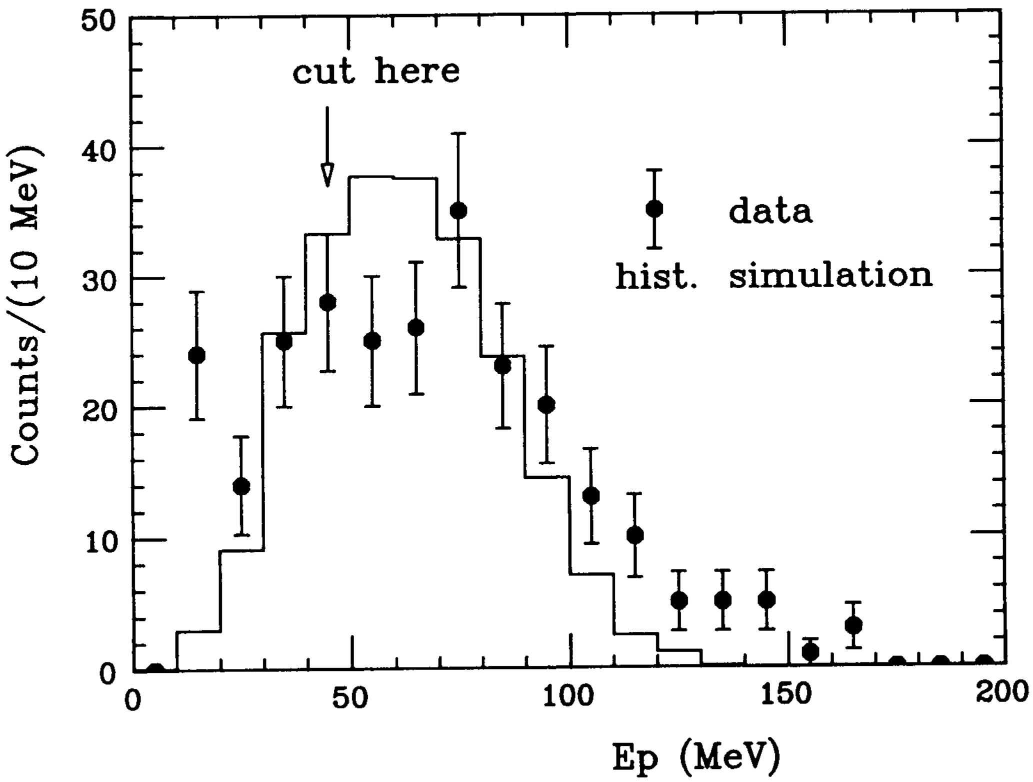

Counts/(10 MeV)
0
10
20
30
40
50
cut here
data
hist. simulation
0
50
100
150
200
Ep (MeV)

Fig. 7

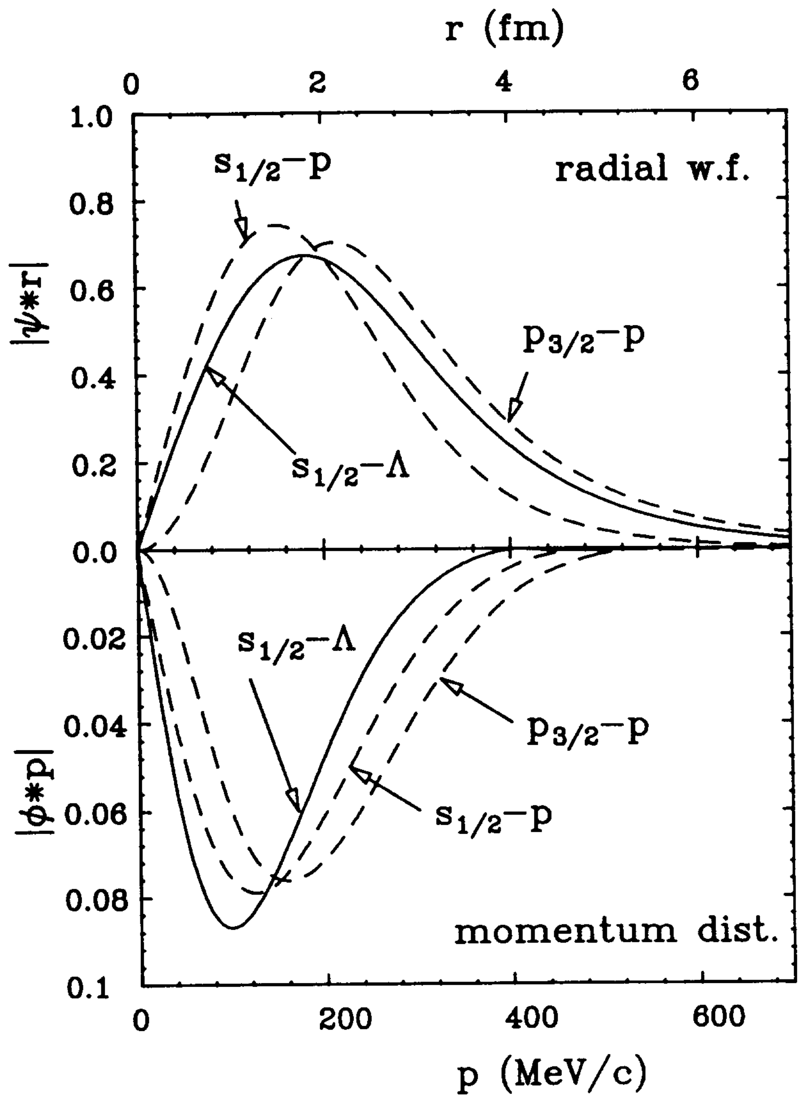

r (fm)
0
2
4
6
1.0
0.8
0.6
0.4
0.2
0.0
0.02
0.04
0.06
0.08
0.1
|ψ*r|
|φ*p|
radial w.f.
$s_{1/2}$−p
$p_{3/2}$−p
$s_{1/2}$−Λ
$s_{1/2}$−Λ
$p_{3/2}$−p
$s_{1/2}$−p
momentum dist.
0
200
400
600
p (MeV/c)

Fig. 8